A figure-eight hysteresis pattern in macroscopic fundamental diagrams and its microscopic causes

Z. He*, S. He and W. Guan

This paper presents macroscopic fundamental diagrams (MFDs) for an urban freeway network in Beijing, China. In the diagrams, a figure-eight hysteresis pattern is observed. To understand the causes, analyses are made ranging from spatiotemporal heterogeneity of vehicles to the flow–occupancy relation for individual locations. Eventually, it is observed at individual locations that free-flow traffic with the same occupancy exhibits different flows in the onset and offset of a rush hour; it is attributed to the counter-clockwise loop in the figure-eight hysteresis pattern at the macroscopic level. Through a simulation scenario based on a cellular automata (CA) model, different lane-changing rates are discussed as the microscopic causes of the flow–occupancy diagram with multiple free-flow branches. In practice, it is inevitable to collect lane-changing data sometimes because of the closeness between detectors and ramps. In the situation, the origin–destination (OD) matrices may influence the shape of MFDs. The paper enriches the knowledge about MFDs and also provides some empirical support for existing theories.

Keywords: Macroscopic fundamental diagram, Hysteresis pattern, Urban freeway network, Lane change

Introduction

Nowadays, most of the approaches of traffic management and control still highly rely on traffic data that are difficult to be obtained sometimes. Combined with complexity of traveler behavior and network topology, the practical effects are compromised. A recently proposed macroscopic fundamental diagram (MFD) for a large urban area provides a new thought on aggregate traffic management and control that are less affected by details.

The MFD reflects invariant macroscopic relationships among space-mean flow, density, and speed in a large urban area. Daganzo and Geroliminis (2008) theoretically proved the existence of the MFD using variational formulation of the kinematic wave theory (Daganzo, 2005a, 2005b) and conjectured four regularity conditions ensuring a well-defined (low scatter) MFD. Meanwhile, Helbing (2009) also derived analytical solutions for the MFD by using a utilization-based approach (Daganzo, 1998). Empirical evidence was provided by Geroliminis and Daganzo (2008), in which a well-defined MFD was first observed for an urban area in Yokohama, Japan.

A number of investigations regarding the MFD were conducted theoretically and practically since the seminal papers were released. In empirical studies, Buisson and Ladier (2009) first reported hysteresis phenomena with clockwise loops existing in an MFD for the Toulouse road network in France and showed that heterogeneity in types and topology of road networks as well as locations of detectors had strong impacts on the shape of the MFD. Geroliminis and Sun (2011a) explicitly investigated causes of the clockwise hysteresis loops by utilizing data collected from the Twin Cities metropolitan area freeway network in Minnesota, USA. Two reasons of the clockwise loops were unveiled: different spatiotemporal distributions of congestion in the onset and offset and synchronized occurrence of capacity drop at individual locations. An association between higher occupancy variance and lower mean flow was also observed. Geroliminis and Sun (2011b) compared the MFDs for the urban areas in Yokohama and Twin Cities, and analyzed characteristics of the road network presenting a well-defined MFD. A sufficient existence condition for a well-defined MFD was addressed. It was also indicated that surface networks more likely exhibited MFDs with low scatter because of the characteristics of network redundancy, traffic signals, etc. Saberi and Mahmassani (2012) explicitly investigated hysteresis patterns in the MFDs for Portland freeway network, USA, and introduced a path-dependent characterization of the

MOE Key Laboratory for Urban Transportation Complex Systems Theory and Technology, Beijing Jiaotong University, Beijing, China

*Corresponding author, email he.zb@hotmail.com

Published by Maney on behalf of the Institute
Received 7 February 2014; accepted 7 September 2014
DOI 10.1179/1942787514Y.0000000041

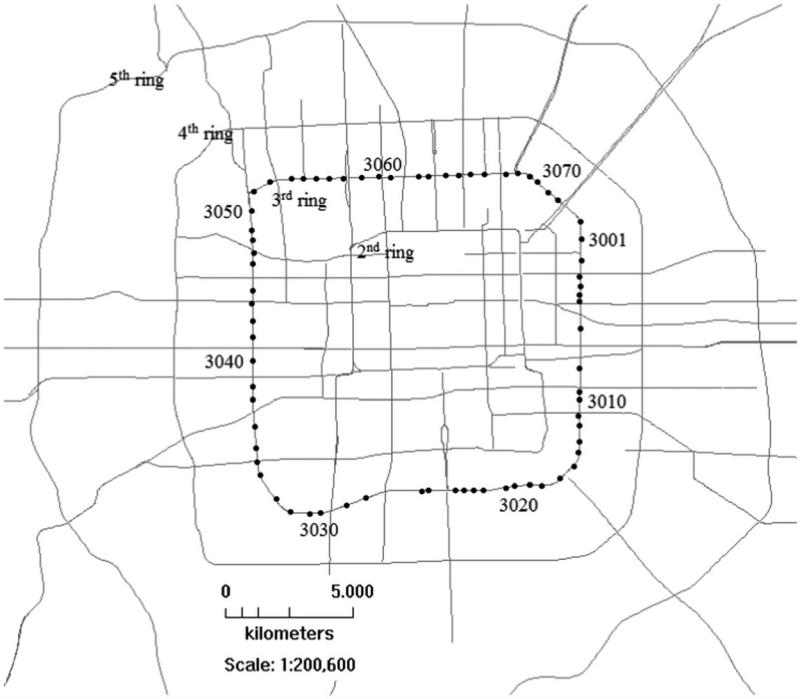

1 The urban freeway network in Beijing and locations of remote transportation microwave sensors (RTMS) on the third urban ring freeway

patterns. Inconstant maximum network flow and different occupancy variations during the recovery period were observed in different days. Saberi and Mahmassani (2013) plotted the MFDs for the freeways in Chicago, Portland, and Irvine, USA. The work characterized the hysteresis loop by its width, height, and covering area, and identified two types of capacity drops. Knoop and Hoogendoorn (2013) proposed a generalized MFD for urban freeways, which relates the production (i.e. the average flow) to the accumulation (i.e. the average number of vehicles in an area) and the spatial spread of density. Ten months of field data of the Amsterdam ring road freeway were used to fit and test the generalized MFD.

In analytical studies, Daganzo (2011) modeled traffic dynamics on a ring freeway with on- and off-ramps by using the kinematic wave theory. The model illustrated how the distribution of flow and density became uneven in the offset of a rush hour even when the ring was symmetric and the demand was uniform. Clockwise hysteresis loops arose with the unevenness. Daganzo and Gayah (2011) modeled a square grid by using a two-ring idealization and further simplified into a two-bin model. The results showed that random turning at intersections aggravated congestion and thereby led to uneven congestion and hysteresis phenomena in the MFD. Gayah and Daganzo (2011) incorporated trip ends into the two-bin model and came to a conclusion that traffic usually exhibited more instability in the offset of a rush hour than in the onset; it also implied that hysteresis phenomena could also arise because of the occurrence of unexpected disturbance even in a symmetric network with uniform demand. Meanwhile, the literature theoretically illustrated a figure-eight hysteresis pattern and stated that the pattern occurred if the loading demand was very unbalanced and the maximum density was quite high; the conditions were rare and no empirical observation has been reported yet.

Based on these studies of the MFD, a variety of applications are proposed recently, such as congestion gating (see, e.g. Haddad and Geroliminis, 2012; Haddad *et al.*, 2013; Keyvan-Ekbatani *et al.*, 2013a, 2013b; Geroliminis *et al.*, 2013) and multimodal traffic management (see, e.g. Gonzales *et al.*, 2010; Zheng and Geroliminis, 2013; Geroliminis *et al.*, 2014). These applications are not explicitly reviewed here, as this paper only focuses on the characteristics of the MFD.

Table 1 All data and the number of ineffective data in each processing step

	Step 1: RTMS data		Step2: lane data		Step 3: data unit		
Date	Total #	Ineff. #	Total #	Ineff. #	Total #	Missing #	Out-range #
June 3	74	9	419	30	280 080	5831(2·08%)	11 345(4·05%)
June 4	74	9	419	26	282 960	8631(3·05%)	11 012(3·90%)
June 5	74	11	407	16	281 520	5359(1·90%)	12 896(4·58%)
June 6	74	9	419	11	293 760	14 600(4·97%)	12 362(4·20%)

RTMS: remote transportation microwave sensors.

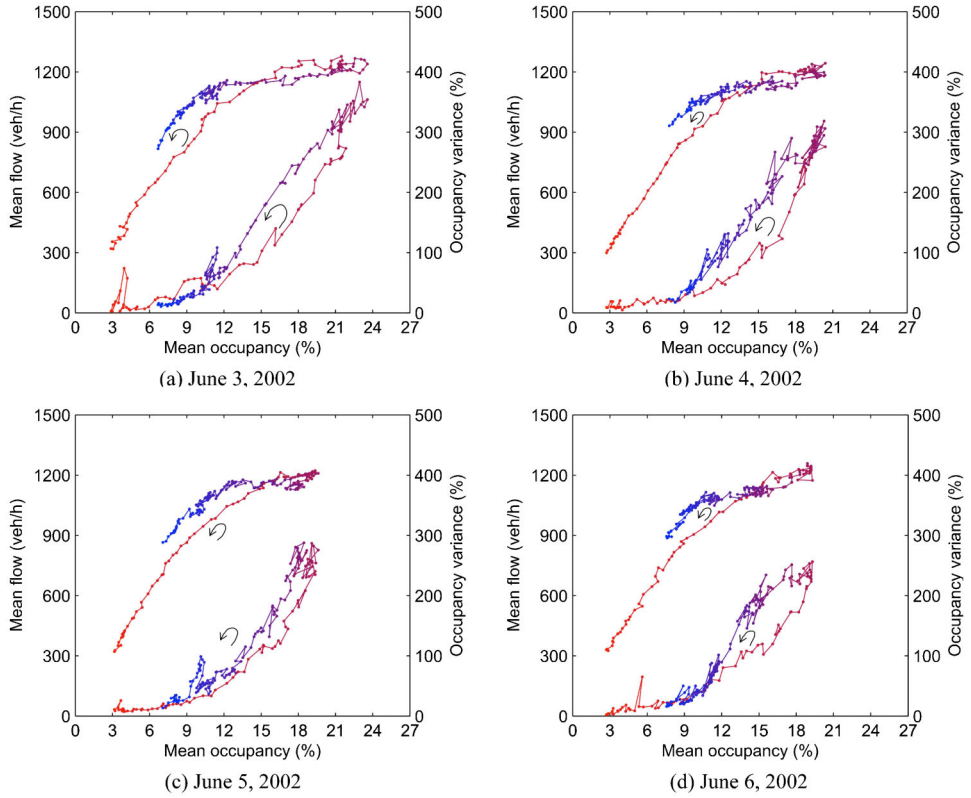

2 Mean flow *v.* mean occupancy (upper plot) and occupancy variance *v.* mean occupancy (lower plot) for the third ring on June 3–6, 2002 (the gradually changing colors from red to blue demonstrate the time growth from 6 : 00 a.m. to 12 : 00 p.m.): *a* June 3, 2002; *b* June 4, 2002; *c* June 5, 2002; *d* June 6, 2002

Understanding the shape and characteristics of an MFD for a network is basic and significant to take advantage of the diagram in practice. In the MFDs for an urban freeway network in Beijing, China, this paper reports a figure-eight hysteresis pattern combining clockwise and counter-clockwise loops, which is only theoretically mentioned in Gayah and Daganzo (2011). Accompanying with the counter-clockwise loop, lower occupancy variance is associated with lower mean flow; it is inconsistent with the observation in Geroliminis and Sun (2011a). The paper is dedicated to reporting the MFDs with the figure-eight hysteresis pattern and to investigating the microscopic causes of the counter-clockwise loop and the association between lower occupancy and lower mean flow. The remainder of the paper is organized as follows: the urban freeway network in Beijing and the data used are presented in the next section; these are followed by a presentation of the figure-eight hysteresis pattern and an investigation of the formation of the counter-clockwise loop; then, the formation of an individual flow–density relation with multiple free-flow branches is discussed based on a cellular automata (CA) model; conclusions are made at last.

Urban freeway network in Beijing and the data

Urban ring freeways in Beijing, China

Beijing is one of the largest cities in the world. At present, four two-way urban ring freeways, i.e. the second–fifth rings, enclose the urban area of Beijing. Among these rings, the third ring with three lanes in each direction is 48·3 km and the speed limits are 80 km h^{-1} for straight sections and 60 km h^{-1} for curves. Seventy-four Remote Transportation Microwave Sensors (RTMS) covering two-way traffic have been installed on the ring (see Fig. 1). Traffic flow data (i.e. occupancy, flow and speed) used in the paper are collected on the ring from 6 a.m. to 12 p.m. on four weekdays, i.e. June 3–6 (Monday–Thursday), 2002. The data are aggregated every 2 min.

Data processing

The data are processed as the following three steps and Table 1 presents the results:

Step 1: Eliminating ineffective RTMS by checking if a data file contains data.

Step 2: Observing the flow–occupancy diagram drawn by using data from each individual lane and discarding entire data pertaining to a lane whose diagram looks obviously incorrect. In this step, the flow–occupancy relation and similarity of the diagrams for adjacent lanes are mainly considered. The step is manual and relies on basic traffic flow knowledge.

Step 3: Removing missing and out-range data. If one item in a data unit of occupancy, flow, and speed at a time slice is out of given intervals, the unit will be removed. The intervals of occupancy, flow, and

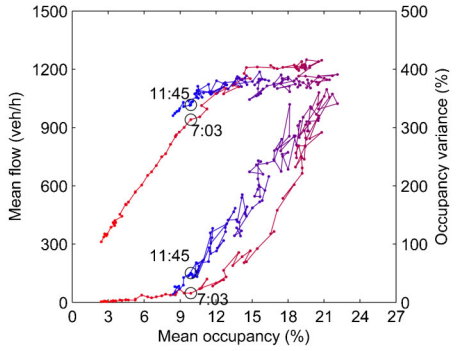

3 Mean flow *v.* mean occupancy (upper plot) and occupancy variance *v* mean occupancy (lower plot) for the counter-clockwise direction in the third ring on June 4, 2002 (the gradually changing colors from red to blue demonstrate the time growth from 6 : 00 a.m. to 12 : 00 p.m.)

speed are chosen as [0,100]%, [0,2500] veh h^{-1}, and [0,100] km h^{-1}, respectively.

Building macroscopic fundamental diagrams

As entire data from some lanes are excluded, this paper takes an average of data of the rest of lanes in a direction covered by a RTMS (this paper regards a direction of each RTMS as a location in the rest of the paper) to represent traffic conditions at the location. Then, the space-mean flow and occupancy on the ring are derived by using the formula introduced in Geroliminis and Daganzo (2008).

Specifically, let i and N be the index and the total number of locations covered by all effective RTMS, respectively, and denote by N_i the number of effective lanes at location i. Occupancy is directly used without being converted to density as usual. Mean flow and mean occupancy at time interval k are obtained as follows

$$Q(k)=\frac{1}{N}\sum_{i=1}^{N}\bar{q}_i(k),\quad \bar{q}_i(k)=\frac{1}{N_i}\sum_{j=1}^{N_i}\alpha_{ij}(k)q_{ij}(k) \tag{1}$$

$$O(k)=\frac{1}{N}\sum_{i=1}^{N}\bar{o}_i(k),\quad \bar{o}_i(k)=\frac{1}{N_i}\sum_{j=1}^{N_i}\beta_{ij}(k)o_{ij}(k) \tag{2}$$

where $q_{ij}(k)$ and $o_{ij}(k)$ are flow and occupancy collected on lane j at location i every 2 min; $\alpha_{ij}(k)$ and $\beta_{ij}(k)\in\{0,1\}$ are dummy coefficients that are equal to 1 if the data unit is effective; 0, otherwise.

Macroscopic fundamental diagrams for the urban freeway network in Beijing

Existence of a figure-eight hysteresis pattern

Macroscopic fundamental diagrams for the four weekdays are built in Fig. 2. Meanwhile, the global variance of occupancy among all locations at a time interval (denoted by $V(k)$) is calculated to represent spatial heterogeneity, and a relation between occupancy variance and mean occupancy is also plotted in Fig. 2.

In Fig. 2, two distinguishing features could be observed: (i) figure-eight hysteresis combining clockwise and counter-clockwise loops and (ii) an association between lower occupancy variance and lower mean flow accompanying with the counter-clockwise loops; it is inconsistent with the observation in Geroliminis and Sun (2011a). The causes of the clockwise loops have been explicitly investigated theoretically and empirically (see, e.g. Buisson and Ladier, 2009; Daganzo, 2011; Geroliminis and Sun, 2011a). Therefore, the remainder of the paper concentrates on the formation of the counter-clockwise loop and the accompanied association.

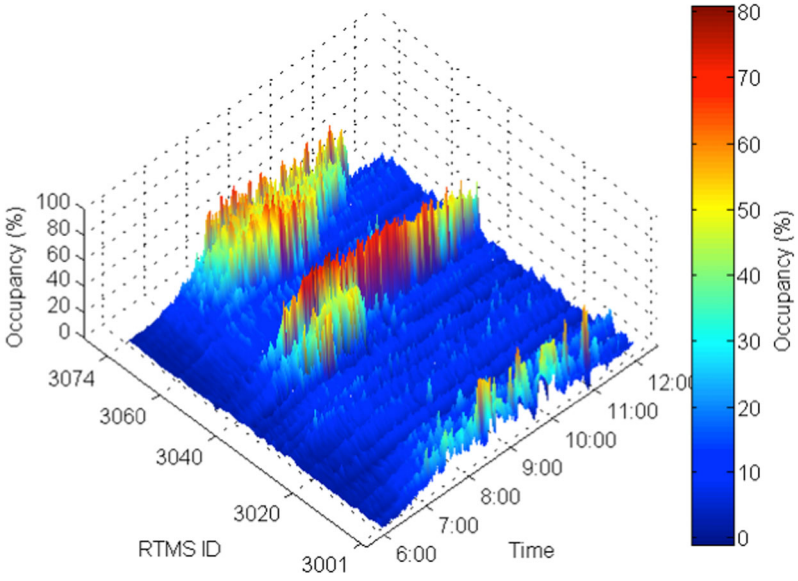

4 spatiotemporal heterogeneity of vehicles in the counter-clockwise direction of the third ring from 6 : 00 a.m. to 12 : 00 p.m. on June 4, 2002

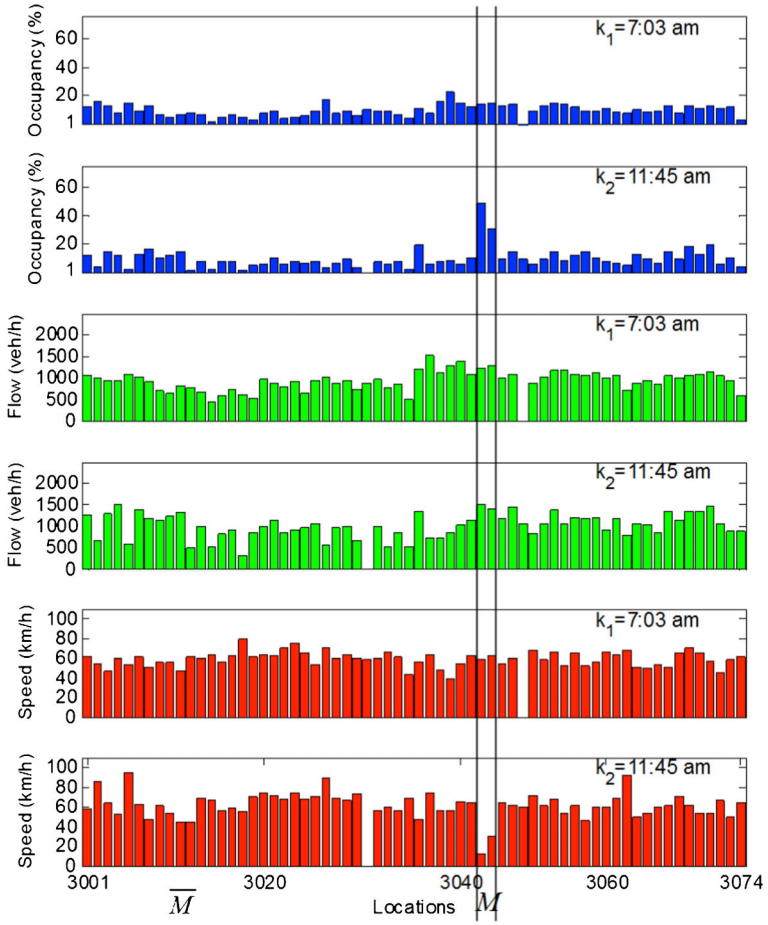

5 Traffic conditions in the two-minute intervals, starting from 7 : 03 and 11 : 45 in the counter-clockwise direction of the third ring on June 4, 2002 (blue, occupancy; green, flow; and red, speed)

Formation of the counter-clockwise loop in the figure-eight hysteresis pattern

This paper selects the counter-clockwise direction of the third ring as an example and deeply look at its spatiotemporal heterogeneity of vehicles (note that there are two directions on a ring road, which are usually called the clockwise and counter-clockwise directions). Figure 3 first shows the relations between mean flow and mean occupancy and between occupancy variance and mean occupancy. In the figure, the aforementioned features are also observed. Figure 4 combines time, locations, and occupancy and provides a clear look at the spatiotemporal heterogeneity. Heavy congestions occur at the locations around 3040 and 3070. The congestion around location 3070 vanishes at the end of the rush hour, while the congestion around location 3040 lasts to the end; it implies higher occupancy variance in the offset of the rush hour.

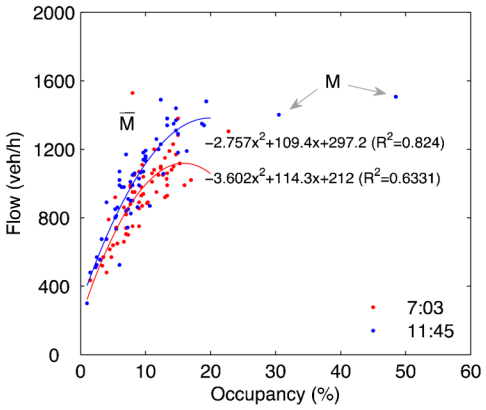

6 Flow *v.* occupancy at all locations at 7 : 03 and 11 : 45 on June 4, 2002 (the curves are fitted using data units which occupancy is lower than 20%)

To see more, this paper selects a pair of 2-min intervals on the counter-clock loop, i.e. k_1 and k_2, which start from 7 : 03 am and from 11 : 45 am, respectively. In the paired time intervals, the mean occupancy is close, while lower occupancy variance is associated with lower mean flow, i.e. $V(k_1) < V(k_2)$ and $Q(k_1) < Q(k_2)$, when $O(k_1) \approx O(k_2)$. Fig. 5 plots the occupancy, flow, and speed in each time interval at all locations. From the figure, two distinguishing traffic conditions can be observed, those are (a) the congested condition existing at location 3042 and 3043 (denoted by M the set of the two locations), where higher occupancy is associated with lower speed comparing with other locations and (b) the free-flow condition at the other locations

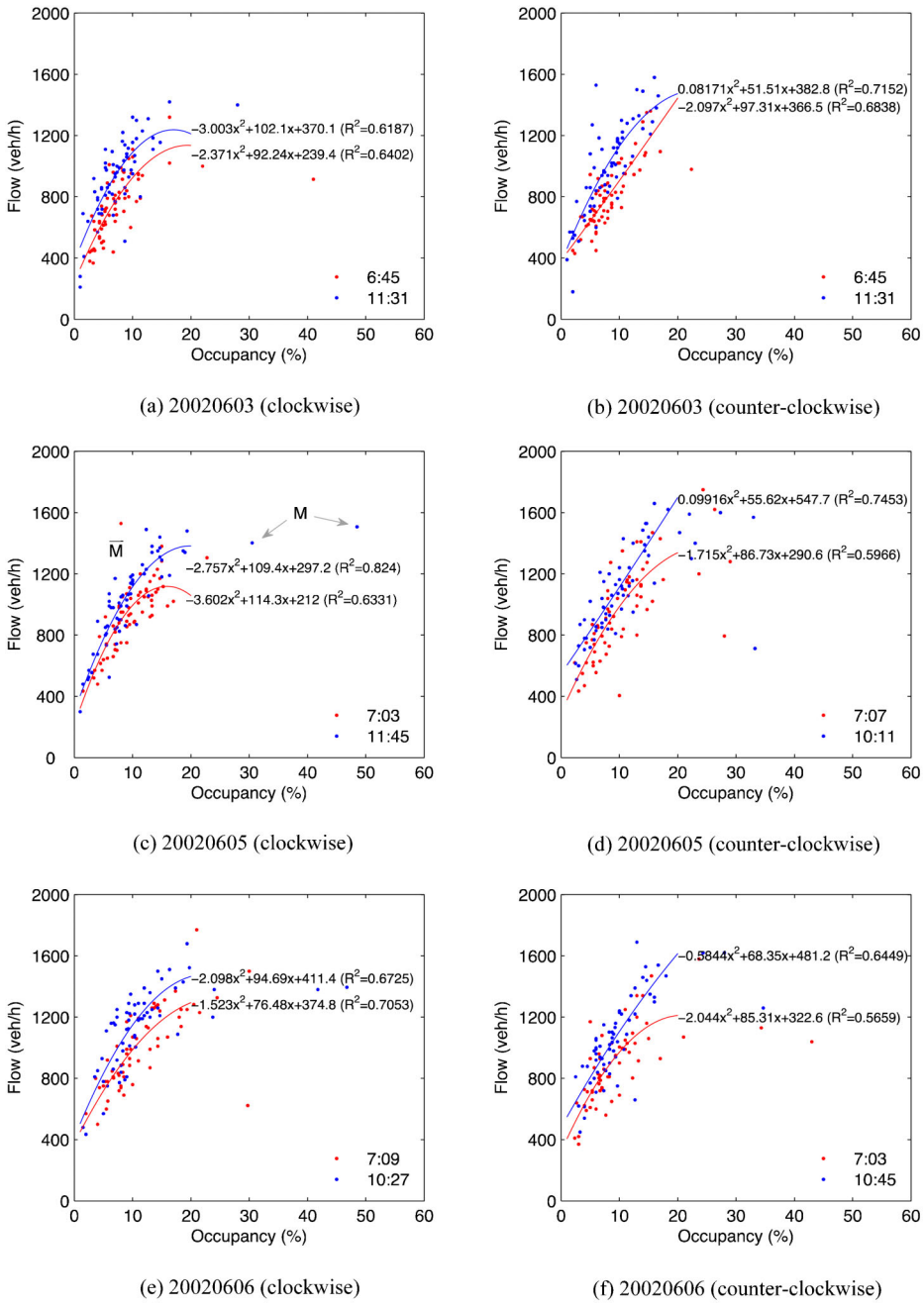

7 Flow *v.* occupancy at all locations at pairs of time slices with the approximate mean occupancy on June 3, 5, and 6, 2002 (the curves are fitted using data units which occupancy is lower than 20%): *a* June 3, 2002 (clockwise); *b* June 3, 2002 (counter-clockwise); *c* June 5, 2002 (clockwise); *d* June 5, 2002 (counter-clockwise); *e* June 6, 2002 (clockwise); *f* June 6, 2002 (counter-clockwise)

(denoted by $\overline{M}$), where all occupancy, speed, and flow are close. The association is now checked.

(i) $V(k_1) < V(k_2)$: From all occupancy in the paired time intervals, it can be seen that all locations are in the free-flow condition in k_1, while congestion still exists at M in k_2. The variance of occupancy in k_2 is thus higher than that in k_1. It is consistent with what existing findings stated.

(ii) $Q(k_1) < Q(k_2)$: The locations of M have

$$\sum_{i \in M} q_i(k_1) \approx \sum_{i \in M} q_i(k_2) \text{ and } \sum_{i \in M} o_i(k_1) < \sum_{i \in M} o_i(k_2) \tag{3}$$

To achieve $Q(k_1) < Q(k_2)$ and simultaneously $O(k_1) \approx O(k_2)$, other locations $\overline{M}$ should have

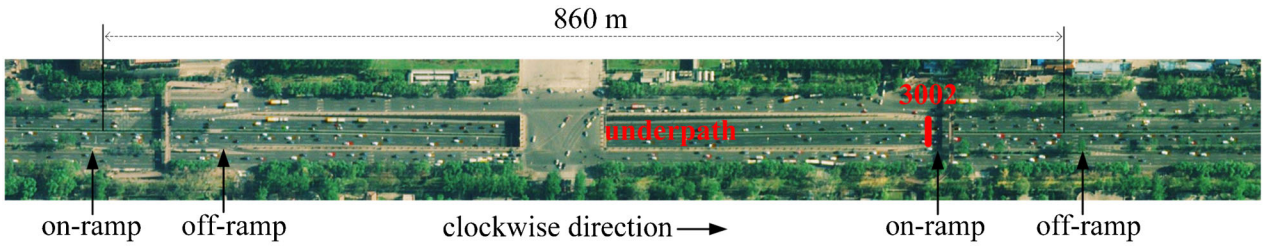

(a) The location of RTMS 3002 in front of National Agriculture Exhibition Center of China

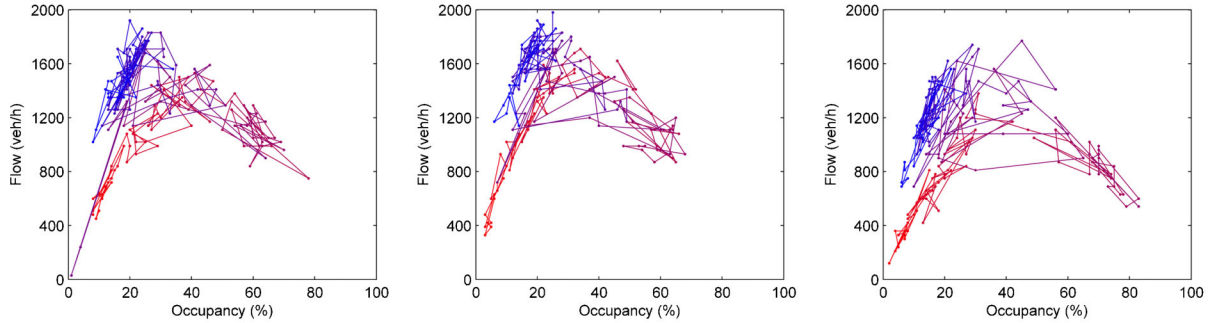

(b) Median lane, clockwise, 3002 (c) Center lane, clockwise, 3002 (d) Shoulder lane, clockwise, 3002

8 Flow–occupancy diagrams for location 3002 on the third ring on June 4, 2002 (the gradually changing colors from red to blue demonstrate the time growth from 6 : 00 a.m. to 12 : 00 p.m.): *a* The location of RTMS 3002 in front of National Agriculture Exhibition Center of China; *b* median lane, clockwise, 3002; *c* center lane, clockwise, 3002; *d* shoulder lane, clockwise, 3002

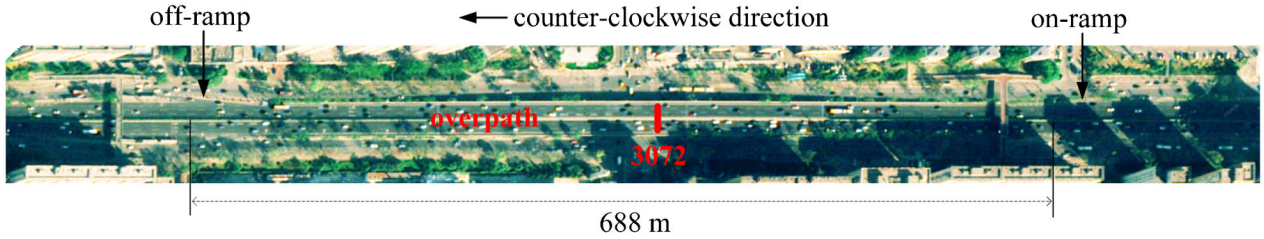

(a) The location of RTMS 3072 on Sanyuan West Bridge

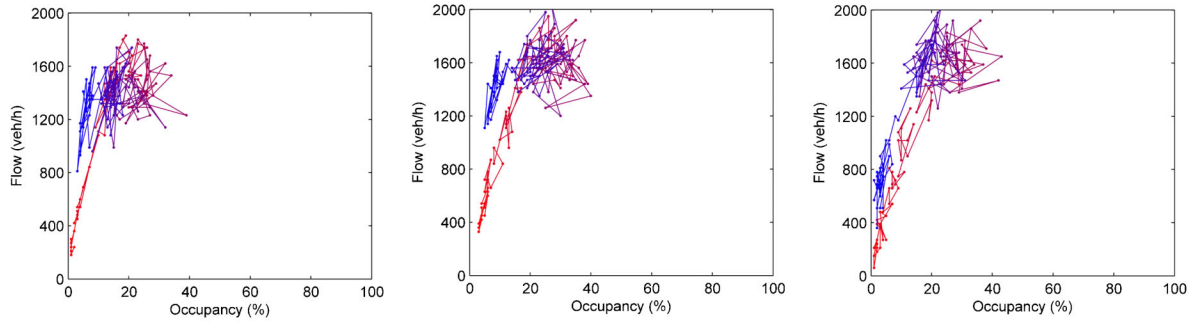

(a) Median lane, counter-clockwise, 3072 (c) Center lane, counter-clockwise, 3072 (d) Shoulder lane, counter-clockwise, 3072

9 Flow–occupancy diagrams for location 3072 on the third ring on June 4, 2002 (the gradually changing colors from red to blue demonstrate the time growth from 6 : 00 a.m. to 12 : 00 p.m.): *a* The location of RTMS 3072 on Sanyuan West Bridge; *b* median lane, counter-clockwise, 3072; *c* center lane, counter-clockwise, 3072; *d* shoulder lane, counter-clockwise, 3072

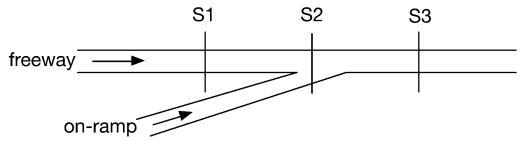

10 A freeway with an on-ramp used for the test

$$\sum_{i\in\overline{M}} q_i(k_1) < \sum_{i\in\overline{M}} q_i(k_2) \text{ and } \sum_{i\in\overline{M}} o_i(k_1) > \sum_{i\in\overline{M}} o_i(k_2) \qquad (4)$$

However, the relations in the figure cannot be seen, and they are rare to the free-flow condition, in which flow and occupancy at an individual location are usually positively correlated as well as the sum of flow and occupancy from different locations based on the fundamental traffic flow theory.

To understand the relations, flow–occupancy relations at different locations in the paired time intervals k_1 and k_2 are plotted in Fig. 6. It can be seen in general that the flow in k_1 is smaller than that in k_2 and the occupancy in k_1 is greater than that in k_2, which lead to inequality (4). It provides insight into the cause of $Q(k_1) < Q(k_2)$ and simultaneously $O(k_1) \approx O(k_2)$. The observation, however, is interesting: in the free-flow condition, the same occupancy in k_1 is associated with lower flow than that in k_2. To show no coincidence, the paper further presents the flow–occupancy relations on other days; see Fig. 7.

To provide more evidences at the microscopic level, this paper plots flow–occupancy diagrams for individual locations and present some of them in Figs. 8 and 9. Two free-flow branches can be seen in the diagrams, i.e. a lower free-flow branch in the onset of the rush hour and a higher branch in the offset. It is interesting and the authors will discuss the causes in the next section. Importantly, note that the speed limits during the selected weekdays were invariant; only a part of the locations exhibit the feature, and the locations in Figs. 8 and 9 are some of

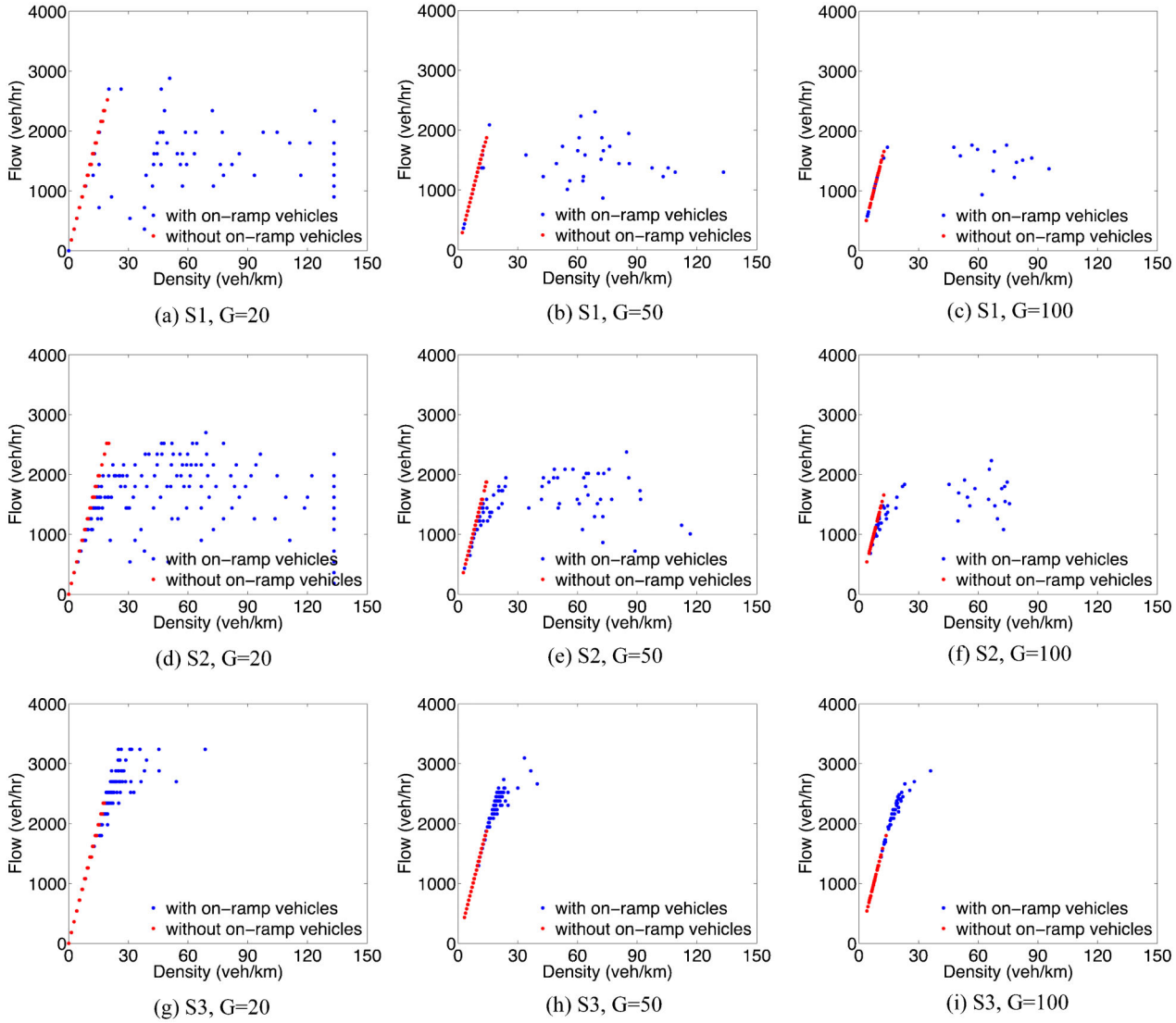

11 The flow–density diagrams for the freeway with an on-ramp (*G* is the size of data aggregation): *a* S1, *G*=20; *b* S1, *G*=50; *c* S1, *G*=100; *d* S2, *G*=20; *e* S2, *G*=50; *f* S2, *G*=100; *g* S3, *G*=20; *h* S3, *G*=50; *i* S3, *G*=100

those with the quite obvious feature. Eventually, this paper considers that the flow–occupancy diagrams with multiple free-flow branches result in the counter-clockwise loop in the figure-eight hysteresis pattern at the macroscopic level.

Discussion of the flow–density diagram with multiple free-flow branches

The urban freeway network in Beijing has unique characteristics, such as a large number of auxiliary roads surrounding and connecting with the urban freeways, dense ramps (a ramp per 0·5 km on average, approximately; refer to Figs. 8*a* and 9*a* for examples), short ramp length, and many interchanges. All of these have significant impact on the traffic and drivers' behavior, in particular the dense ramps, which result in frequent lane-changing maneuvers. It is conjectured that the lower free-flow branch is caused by higher lane-changing rates, and verify it in the following simulation scenario based on the well-known CA model proposed by Nagel and Schreckenberg (1992) (see Appendix for the CA model).

The simulation network is composed of a one-lane freeway with an on-ramp (see Fig. 10). Vehicles on the on-ramp are forced to change to the freeway at the end of the on-ramp. Before updating vehicles following the CA model, vehicles at the end of the on-ramp move sideways to the freeway regardless of the traffic condition in the freeway. The approaching vehicles in the freeway thus have to brake when a vehicle merges from the on-ramp. No crash will be triggered, which is guaranteed by the CA model in the freeway (see, e.g. Rickert *et al.*, 1996; Chowdhury *et al.*, 1997).

At each simulation step, vehicles are loaded on the beginning of the freeway and ramp with a probability. Three probabilities of 0·2, 0·25, and 0·3 are selected. Each of the probabilities is implemented for 1500 simulation steps. The free-flow speed is set to be 5 cell/step (i.e. 135 km h^{-1} if the length of a cell is 7·5 m), and the slowdown probability be 0·2. Data used to plot the flow–density diagram are collected from three detection locations, i.e. S1, S2, and S3 (see Fig. 10). The distances between two adjacent locations are 20 cells. Only the data collected from S2 are influenced by the lane change.

The flow–density diagrams with and without the influence of on-ramp vehicles are compared in Fig. 11. It can be seen that the red spots in all subfigures and the free-flow parts of the blue spots for S1 and S3 (Fig. 11*a–c* and *g–i*) exhibit only one branch. It turns out that there is one free-flow branch in the flow–density diagram when lane change does not exist. In contrast, the lane change results in a lower free-flow branch in the blue spots for S2 (Fig. 11*d–f*). This confirms the conjecture that higher lane-changing rates result in the lower free-flow branch, and vice versa.

It is known that the lane-changing rates are closely related to inflow and outflow via on- and off-ramps as well as the origin–destination (OD) matrices. In an urban freeway network with dense ramps, like the urban freeways in Beijing, it is difficult to avoid locating detectors in the vicinity of ramps, and more lane-changing maneuvers are thus included in the detected traffic flow data. In the situation, the OD matrices may influence the shape of MFDs.

Conclusion

A figure-eight hysteresis pattern is observed in the MFDs for the third urban ring freeway in Beijing, China. To understand the microscopic causes, analyses are made ranging from spatiotemporal heterogeneity of vehicles to the flow–occupancy relation for individual locations. At individual locations, it is observed that the free-flow traffic with the same occupancy exhibits lower flow in the onset of the rush hour and higher flow in the offset. The observation is unveiled to be the results of the counter-clockwise loop in the figure-eight hysteresis pattern and the association between lower occupancy variance and lower mean occupancy.

To better understand the flow–density diagram with multiple free-flow branches, a freeway with an on-ramp is simulated using the well-known CA model. It is clearly shown that higher lane-changing rates result in a lower free-flow branch and vice versa. It confirms the influence of lane-changing rates to the flow–density diagram. In practice, locating detectors closely to ramps may be difficult to be avoided in an urban freeway network with dense ramps. In the situation, the OD matrices, which may result in different lane-changing rates in different times, could influence the shape of MFDs.

Moreover, this paper empirically presents the MFDs for an urban ring freeway. The hysteresis phenomena are also observed in the MFDs for the urban freeway network with more ramps (i.e. there are more route choices for drivers than those in regular freeways).

Appendix: A cellular automata traffic model

The cellular automata (CA) traffic model (Nagel and Schreckenberg, 1992) divides a road into L cells, which can be either empty or occupied by a vehicle. The simulation at discrete time step is updated in parallel as follows

$$\begin{aligned}
&\text{(1)Acceleration :} && v_n \rightarrow \min\{v_n+1, v_{\max}\}\\
&\text{(2)Safety distance :} && v_n \rightarrow \min\{v_n, d_n\}\\
&\text{(3)Randomization :} && v_n \rightarrow \max\{v_n-1, 0\}\\
&\text{with probability } p_{\text{slow}} && \\
&\text{(4)Moving :} && x_n \rightarrow x_n + d_n
\end{aligned} \tag{A1}$$

where $v_n = 0,1,\ldots,v_{\max}$ is the velocity of vehicle n, d_n is the number of empty cells in front of vehicle n, p_{slow} is a slowdown probability, and x_n is the position of vehicle n.

Acknowledgement

This research has been funded by 973 program (2012CB725403) and Beijing Science and Technology Commission Foundation (Z131110002813118).

References

Buisson, C. and Ladier, C. 2009. Exploring the impact of homogeneity of traffic measurements on the existence of macroscopic fundamental diagrams, *J Transp Res Board*, (2124), 127–136.

Chowdhury, D., Wolf, D. E. and Schreckenberg, M. 1997. Particle hopping models for two-lane traffic with two kinds of vehicles: effects of lane-changing rules, *Physica A: Stat Mech Appl*, **235**, 417–439.

Daganzo, C. 1998. Queue spillovers in transportation networks with a route choice, *Transp Sci*, **32**, 3–11.

Daganzo, C. 2005a. A variational formulation of kinematic waves: solution methods, *Transp Res B: Methodol*, **39**, 934–950.

Daganzo, C. and Gayah, V. 2011. Macroscopic relations of urban traffic variables: bifurcations, multivaluedness and instability, *Transp Res B: Methodol*, **45**, 278–288.

Daganzo, C. F. 2005b. A variational formulation of kinematic waves: basic theory and complex boundary conditions, *Transp Res B: Methodol*, **39**, 187–196.

Daganzo, C. F. 2011. On the macroscopic stability of freeway traffic, *Transp Res B: Methodol*, **45**, 782–788.

Daganzo, C. F. and Geroliminis, N. 2008. An analytical approximation for the macroscopic fundamental diagram of urban traffic, *Transp Res B: Methodol*, **42**, 771–781.

Gayah, V. V. and Daganzo, C. F. 2011. Clockwise hysteresis loops in the macroscopic fundamental diagram: an effect of network instability, *Transp Res B: Methodol*, **45**, 643–655.

Geroliminis, N. and Daganzo, C. F. 2008. Existence of urban-scale macroscopic fundamental diagrams: some experimental findings, *Transp Res B: Methodol*, **42**, 759–770.

Geroliminis, N., Haddad, J. and Ramezani, M. 2013. Optimal perimeter control for two urban regions with macroscopic fundamental diagrams: a model predictive approach, *IEEE Trans Intel Transp Syst*, **14**, 348–359.

Geroliminis, N. and Sun, J. 2011a. Hysteresis phenomena of a macroscopic fundamental diagram in freeway networks, *Transp Res A: Policy Practice*, **45**, 966–979.

Geroliminis, N. and Sun, J. 2011b. Properties of a well-defined macroscopic fundamental diagram for urban traffic, *Transp Res B: Methodol*, **45**, 605–617.

Geroliminis, N., Zheng, N. and Ampountolas, K. 2014. A three-dimensional macroscopic fundamental diagram for mixed bi-modal urban networks, *Transp Res C: Emerg Technol*, **42**, 168–181.

Gonzales, E. J., Geroliminis, N., Cassidy, M. J. and Daganzo, C. F. 2010. On the allocation of city space to multiple transport modes, *Transp Plann Technol*, **33**, 643–656.

Haddad, J. and Geroliminis, N. 2012. On the stability of traffic perimeter control in two-region urban cities, *Transp Res B: Methodol*, **46**, 1159–1176.

Haddad, J., Ramezani, M. and Geroliminis, N. 2013. Cooperative traffic control of a mixed network with two urban regions and a freeway, *Transp Res B: Methodol*, **54**, 17–36.

Helbing, D. 2009. Derivation of a fundamental diagram for urban traffic flow, *Eur. Phys. J. B*, **70**, 229–241.

Keyvan-Ekbatani, M., Papageorgiou, M. and Papamichail, I. 2013a. Urban congestion gating control based on reduced operational network fundamental diagrams, *Transp Res C: Emerg Technol*, **33**, 74–87.

Keyvan-Ekbatani, M., Yildirimoglu, M., Geroliminis, N. and Papageorgiou, M. 2013b. The Hague, The Netherlands, Traffic signal perimeter control with multiple boundaries for large urban networks, in 16th International IEEE Conference on Intelligent Transportation Systems (ITSC 2013), 1004–1009, IEEE, The Hague, The Netherlands.

Knoop, V. L. and Hoogendoorn, S. 2013. Empirics of a generalized macroscopic fundamental diagram for urban freeways, Knoop, V. L. and Hoogendoorn, S, 2013. Empirics of a generalized macroscopic fundamental diagram for urban freeways, J Transp Res Board. 2391, 133–141.

Nagel, K. and Schreckenberg, M. 1992. A cellular automation model for freeway traffic, *J. Phys. I*, **2**, 2221–2229.

Rickert, M., Nagel, K., Schreckenberg, M. and Latour, A. 1996. Two lane traffic simulations using cellular automata, *Physica A: Stat Mech Appl*, **231**, (4), 534–550.

Saberi, M. and Mahmassani, H. S. 2012. Exploring properties of networkwide flow–density relations in a freeway network, *Transp Res Record*, **2315**, 153–163.

Saberi, M. and Mahmassani, H. S. 2013. Hysteresis and capacity drop phenomena in freeway networks: empirical characterization and interpretation, *Transp Res Record*, **2391**, 44–55.

Zheng, N. and Geroliminis, N. 2013. On the distribution of urban road space for multimodal congested networks, *Transp Res B: Methodol*, **57**, 326–341.